7086 *Inorg. Chem.* **2009**, *48*, 7086–7098
DOI: 10.1021/ic8023277

Inorganic Chemistry
Article

Structural, UV−Visible, and Electrochemical Studies on 2,3-Dicyano-5,6-di-2-pyridylpyrazine, $[(CN)_2Py_2Pyz]$, Related Species and Its Complexes $[(CN)_2Py_2PyzMCl_2]$ (M = Pt^{II}, Pd^{II})

Xiaohui Cai,[†] Maria Pia Donzello,*[,‡] Elisa Viola,[‡] Corrado Rizzoli,[§] Claudio Ercolani,[‡] and Karl M. Kadish*[,†]

[†]*Department of Chemistry, University of Houston, Houston, Texas 77204-5003,* [‡]*Dipartimento di Chimica, Università degli Studi di Roma "La Sapienza", Piazelle A. Moro 5, I-00185 Rome, Italy, and* [§]*Dipartimento di Chimica Generale ed Inorganica, Università di Parma, viale G. P. Usberti 17-A, I-43100 Parma, Italy*

Received December 4, 2008

2,3-Dicyano-5,6-di-2-pyridylpyrazine, $[(CN)_2Py_2Pyz]$, which autocyclotetramerizes to give the macrocycle tetrakis[5,6-di(2-pyridyl)-2,3-pyrazino]porphyrazine, $[Py_8TPyzPzH_2]$, bearing externally four dipyridinopyrazine fragments, reacts with bis(benzonitrile)dichloroplatinum(II), $[(C_6H_5CN)_2PtCl_2]$, in CH_3CN, affording the monometalated species $[(CN)_2Py_2PyzPtCl_2]$. Single-crystal X-ray work on this compound shows that Pt^{II} is bound to $[(CN)_2Py_2Pyz]$ through the two pyridine N atoms ("py−py" coordination) in a way similar to that found for its monopalladium analogue, $[(CN)_2Py_2PyzPdCl_2]$. Cyclic voltammetry of $[(CN)_2Py_2PyzPtCl_2]$ and $[(CN)_2Py_2PyzPdCl_2]$ in nonaqueous media (pyridine, DMSO, and DMF) indicates that the electron-withdrawing effect of the coordinated $PtCl_2$ and $PdCl_2$ units results in an initial one-electron reduction ($E_{1/2}$ = −0.60 and −0.54 V vs SCE in DMSO, respectively), which is easier by 0.25−0.30 V than the unmetalated $[(CN)_2Py_2Pyz]$ (first reduction: $E_{1/2}$ = −0.87 V vs SCE). These electrochemical data are analyzed along with new results for a selected number of related pyrazine and 2,3-dicyanopyrazine molecules as well as earlier reported data on the mono- and bis-N-methylated derivatives $[(CN)_2Py(2\text{-}Mepy)Pyz]^+$ and $[(CN)_2(2\text{-}Mepy)_2Pyz]^{2+}$, with these latter species being formed by reaction of the precursor $[(CN)_2Py_2Pyz]$ with methyl iodide or *p*-toluensulfonate. The data in this study are also compared to electrochemical data previously reported for a triad of palladium(II) porphyrazine macrocycles obtained from the precursor $[(CN)_2Py_2Pyz]$, i.e., $[Py_8TPyzPzPd]$, the corresponding pentanuclear complex $[(PdCl_2)_4Py_8TPyzPzPd]$ (presenting "py−py" coordination at the dipyridinopyrazine fragments), and the octacation $[(2\text{-}Mepy)_8TPyzPzPd]^{8+}$ (N-methylated at the pyridine rings). Thin-layer UV−visible spectra of singly reduced $[(CN)_2Py_2Pyz]^-$ and its metalated analogues, $[(CN)_2Py_2PyzPtCl_2]^-$ and $[(CN)_2Py_2PyzPdCl_2]^-$, were measured in pyridine, DMF, and DMSO and show $\pi-\pi^*$ transitions, as well as unusually intense absorptions in the near-IR region (500−900 nm) of the spectrum.

Introduction

In an earlier study, it was reported that the free-base macrocycle tetrakis[5,6-di(2-pyridyl)-2,3-pyrazino]porphyrazine, $[Py_8TPyzPzH_2]$ (Chart 1A), bearing peripherally annulated dipyridinopyrazine fragments, is easily formed by autocyclotetramerization of the precursor 2,3-dicyano-5,6-di-2-pyridyl-1,4-pyrazine, $[(CN)_2Py_2Pyz]$.[1] Detailed electrochemical and spectroelectrochemical investigations of $[Py_8TPyzPzH_2]$,[1] its metal derivatives $[Py_8TPyzPzM]$[2a,2c] (M= $Mg^{II}(H_2O)$, Mn^{II}, Co^{II}, Cu^{II}, Zn^{II}), and the related octacations $[(2\text{-}Mepy)_8TPyzPzM]^{8+}$ (M = $2H^1$; Chart 1B)[2b,2c] were previously carried out in pyridine and dimethyl sulfoxide (DMSO).[1,2] Each compound was shown to undergo reversible well-separated one-electron reductions, with the formation of 1−, 2−, 3−, and 4− charged species, at potentials significantly less negative than those for the reduction of their phthalocyanine analogues. The facile reductions are strictly related to the electron-deficient properties of the porphyrazine framework $Py_8TPyzPz$ as determined by the contributing effect of the electronegative *meso*-N atoms and the overall electron-attracting properties of the external dipyridinoyrazine fragments carrying pyrazine N and external pyridine N atoms. Moreover, recent work from our laboratory also demonstrated that conversion of the mononuclear Pd^{II} complex $[Py_8TPyzPzPd]$ to its singly reduced $[Py_8TPyzPzPd]^-$ form (first reduction at −0.26 V vs SCE in DMSO) is made even easier by exocyclic "py−py" coordination of four $PdCl_2$ units.[3] In fact, the

*To whom correspondence should be addressed. E-mail: kkadish@uh.edu (K.M.K.), mariapia.donzello@uniroma1.it (M.P.D.).

(1) Donzello, M. P.; Ou, Z.; Monacelli, F.; Ricciardi, G.; Rizzoli, C.; Ercolani, C.; Kadish, K. M. *Inorg. Chem.* **2004**, *43*, 8626.

(2) (a) Donzello, M. P.; Ou, Z.; Dini, D.; Meneghetti, M.; Ercolani, C.; Kadish, K. M. *Inorg. Chem.* **2004**, *43*, 8637. (b) Bergami, C.; Donzello, M. P.; Ercolani, C.; Monacelli, F.; Kadish, K. M.; Rizzoli, C. *Inorg. Chem.* **2005**, *44*, 9852. (c) Bergami, C.; Donzello, M. P.; Monacelli, F.; Ercolani, C.; Kadish, K. M. *Inorg. Chem.* **2005**, *44*, 9862.

(3) Donzello, M. P.; Viola, E.; Cai, X.; Mannina, L.; Rizzoli, C.; Ricciardi, G.; Ercolani, C.; Kadish, K. M.; Rosa, A. *Inorg. Chem.* **2008**, *47*, 3903.

 Published on Web 07/07/2009 © 2009 American Chemical Society

Chart 1. Schematic Representation of the Unmetalated Tetrakis[5,6-di(2-pyridyl)-2,3-pyrazino]porphyrazine, [$Py_8TPyzPzH_2$] (A) and Its Corresponding Octacation [$(2\text{-Mepy})_8TPyzPzH_2]^{8+}$ (B)

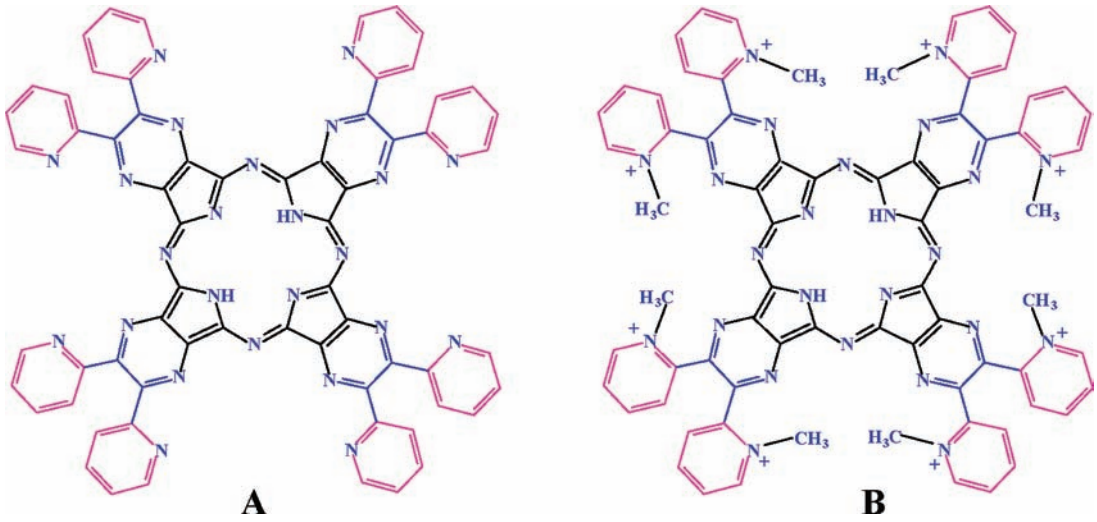

pentanuclear species [$(PdCl_2)_4Py_8TPyzPzPd$] undergoes an initial macrocycle-centered reduction at 0.00 V vs SCE under the same experimental conditions, a positive shift of 260 mV.

A facile uptake of electrons is also observed to occur after quaternization of the eight pyridine N atoms of [$Py_8TPyzPzM$] ($M = Mg^{II}(H_2O)$, Mn^{II}, Co^{II}, Cu^{II}, Zn^{II}), leading to the corresponding 8+ charged species[2c,3] [$(2\text{-Mepy})_8TPyzPzM]^{8+}$ and parallel easier reductions that are also seen for [$Py_8TPyzPzPd$] and [$(2\text{-Mepy})_8TPyzPzPd]^{8+}$, with the latter species undergoing a one-electron addition at $E_{1/2} = 0.08$ V, fully 340 mV easier than that for reduction of [$Py_8TPyzPzPd$].

In view of our continuing work on the synthesis and physicochemical studies of homo- and heteronuclear porphyrazine macrocycles carrying peripherally annulated di-2-pyridylpyrazine substituents, it was believed to be useful to investigate the electrochemical and spectroscopic properties of the ligated and unligated di-2-pyridylpyrazine moiety as well as reexamine the *N*-pyridine quaternized derivatives in the absence of the porphyrazine macrocycle. This is done in the present study, which describes the synthesis and structural characterization of the monoplatinated complex [$(CN)_2Py_2PyzPtCl_2$] formed in a reaction involving [$(C_6H_5CN)_2PtCl_2$] and [$(CN)_2Py_2Pyz$], the latter of which is a precursor of the porphyrazine macrocycles (Chart 1A). The electrochemical properties and spectroscopic characterization of the singly reduced precursor [$(CN)_2Py_2Pyz$], and two corresponding metalated complexes, [$(CN)_2Py_2PyzMCl_2$] ($M = Pt^{II}$, Pd^{II}), are also investigated. These electrochemical data are then combined with previous results on the related mono- and bis-N-methylated cations [$(CN)_2Py(2\text{-Mepy})Pyz]^+$ and [$(CN)_2(2\text{-Mepy})_2Pyz]^{2+}$ which are formed upon quaternization with methyl iodide or *p*-toluensulfonate of the precursor [$(CN)_2Py_2Pyz$]. The overall spectroscopic and electrochemical data provide additional information on the role played by the dipyridinopyrazine fragments when included as peripherally annulated residues in macrocyclic porphyrazine systems and also lead to a better understanding of the electronic effects of exocyclic metal coordination as well as the effect of a positive charge location on the external pyridine N atoms (quaternization). As will be illustrated, a spectroelectrochemical investigation of singly reduced [$(CN)_2Py_2Pyz$], [$(CN)_2Py_2PyzPtCl_2$], and [$(CN)_2Py_2PyzPdCl_2$] shows the presence of intense absorptions in the region 500−900 nm. To better understand these spectra, our electrochemical and spectroelectrochemical studies were also extended to include a selected number of related neutral species, and the results of this study are also reported in the present paper.

Experimental Section

Solvents and Reagents. Solvents and reagents were commercially available materials and were used as received. 2,3-Dicyano-5,6-di-2-pyridylpyrazine, [$(CN)_2Py_2Pyz$],[1] and [$(CN)_2Py_2PyzPdCl_2$][3] were prepared as previously reported. 2,3-Dicyano-5,6-di-2-thienylpyrazine, [$(CN)_2Th_2Pyz$],[4] 2,3-dicyano-5,6-diphenylpyrazine, [$(CN)_2Ph_2Pyz$],[5] and 2,3-dicyano-5,6-dimethylpyrazine, [$(CN)_2(CH_3)_2Pyz$],[6] were prepared as described elsewhere. 2,3-Dicyanopyrazine, [$(CN)_2Pyz$], and 2,3-dipyridinopyrazine, [Py_2Pyz], were commercial products (Aldrich). The mono- and bis-N-methylated 1+ and 2+ charged species [$(CN)_2Py(2\text{-Mepy})Pyz]^+$ and [$(CN)_2(2\text{-Mepy})_2Pyz]^{2+}$, neutralized by the iodide or *p*-toluensulfonate anion, $CH_3C_6H_4SO_3^-$, were obtained as reported earlier.[2b] Bis(benzonitrile)dichloroplatinum(II), [$(C_6H_5CN)_2PtCl_2$], was prepared according to a procedure reported in the literature for synthesis of the Pd^{II} analogue, [$(C_6H_5CN)_2PdCl_2$].[7]

Synthesis of [$(CN)_2Py_2PyzPtCl_2$]. A solution of [$(C_6H_5CN)_2PtCl_2$] (244 mg, 1.08 mmol) and 2,3-dicyano-5,6-di-2-pyridyl-1,4-pyrazine, [$(CN)_2Py_2Pyz$] (141.6 mg, 0.497 mmol), in CH_3CN (30 mL) was heated at 70 °C and maintained at this temperature for 2 h. After cooling and concentration of the solution, the resulting light-yellow crystals were filtered off, washed with CH_3CN, and brought to a constant weight under vacuum (10^{-2} mmHg) (121.4 mg, yield 44.3%). Calcd for [$(CN)_2Py_2PyzPtCl_2$], $C_{16}H_8Cl_2N_6Pt$: C, 34.92; H, 1.47; N, 15.27; Pt, 35.45. Found: C, 35.81; H, 2.02; N, 15.99; Pt, 34.18. IR (KBr, cm^{-1}) (Figure S1 in the Supporting Information, SI): ca. 3500 w (very broad), 3109 vw, 3076 w, 2334 vvw, 2287 vvw, 2249 vw, 1601 m, 1570 vvw, 1524 vw, 1489 m, 1439 w-m, 1383 vs,

(4) Morkved, E. H.; Ossletten, H.; Kjosen, H. *J. Prakt. Chem.* **2000**, *342*, 83.
(5) Bauer, E. M.; Ercolani, C.; Galli, P.; Popkova, I. A.; Stuzhin, P. A. *J. Porphyrins Phthalocyanines* **1999**, *3*, 371.
(6) Rothkopf, H. W.; Wöhrle, D.; Müller, R.; Kossmehl, G. *Chem. Ber.* **1975**, *108*, 875.
(7) Kharasch, M. S.; Seyler, R. C.; Mayo, F. R. *J. Am. Chem. Soc.* **1938**, *60*, 882.

Table 1. Crystallographic Data for $[(CN)_2Py_2PyzPtCl_2]$

formula	$C_{16}H_8Cl_2N_6Pt \cdot 0.875C_2H_3N$
a, Å	11.5966(6)
b, Å	13.0168(7)
c, Å	28.4197(16)
β, deg	100.4777(10)
V, Å^3	4218.4(4)
Z	8
fw	586.20
space group	$P2_1/c$
T, °C	22
λ, Å	0.710 73
ρ_{calc}, g cm^{-3}	1.846
μ, mm^{-1}	6.922
transmn coeff	0.443−0.707
R1[a]	0.039
wR2	0.071
GOF	1.009
no. of obsd reflns[b]	4704
no. of indep reflns[c]	7467
no. of refinement reflns[d]	7467
no. of variables	505

[a] Calculated on the observed reflections having $I > 2\sigma(I)$. [b] Number of the independent reflections having $I > 2\sigma(I)$. [c] Number of independent reflections. [d] Number of reflections used in the refinement having $I > 0$.

1286 m, 1252 m, 1242 w-m, 1196 w-m, 1163 w, 1142 vw, 1130 vvw, 1113 vvw, 1095 w-m, 1067 m, 1038 vw, 918 vvw, 895 vw, 841 vvw, 825 w, 814 w-m, 785 s, 764 m-s, 758 m-s, 698 w, 685 vw, 662 w, 571 m, 548 vw, 532 w-m, 492 vvw, 442 vw, 380 vw, 350, 340 m/split ν_{Pt-Cl}. The complex gave crystals suitable for X-ray analysis after recrystallization from hot CH_3CN.

X-ray Crystallography of $[(CN)_2Py_2PyzPtCl_2]$. Crystal data and details associated with structure refinement are given in Table 1 and in the SI (Tables S1 and S2). The data were collected on a Bruker SMART 1000 CCD diffractometer using graphite-monochromatized Mo Kα (radiation at 295 K). The solution and refinement were carried out using the programs *SIR97*[8] and *SHELX97*.[9]

^{1}H NMR. ^{1}H NMR spectra were taken in *N*,*N*-dimethylformamide (DMF; 99.5% DMF-d_7 CIL, 0.4 mL) at 300 K with a Bruker AVANCE AQS600 spectrometer operating at the ^{1}H frequency of 600.13 MHz and equipped with a Bruker multinuclear *z*-gradient inverse probehead capable of producing gradients in the *z* direction with a strength of 55 G cm^{-1}. The ^{1}H NMR spectra were obtained using 32K data points, a recycle delay of 8 s, and a 90° flip angle pulse of 9 μs. The ^{1}H−^{1}H gradient-selected COSY-45 experiments were recorded using the following acquisition and processing parameters: a spectral width of 12 ppm in both dimensions, 4096 data points in the f2 dimension, 256 increments in the f1 dimension, a relaxation delay of 2 s, 16 dummy scans, and 200 scans; data were processed in magnitude mode with 8192 × 1024 data points. Chemical shifts were referred to the residual singlet proton (8.03 ppm) of DMF-d_7.

Electrochemical Measurements. Cyclic voltammetry was carried out with an EG&G model 173 potentiostat coupled to an EG&G model 175 universal programmer. Current−voltage curves were recorded on an EG&G Princeton Applied Research model R-0151 *X*−*Y* recorder. A three-electrode system was used, consisting of a glassy carbon working electrode, a platinum counter electrode, and a saturated calomel reference electrode (SCE). UV−visible spectroelectrochemical experiments were carried out with a homemade thin-layer cell that had a light-transparent platinum gauze working electrode.[10] Potentials were applied and monitored with an EG&G model 173 potentiostat.

UV−visible spectra were recorded on a Hewlett-Packard model 8453 diode array spectrophotometer. Solvents for the electrochemical measurements were pyridine (99.9+%), dimethyl sulfoxide (DMSO; 99.9+%), and *N*,*N*-dimethylformamide (DMF; 99.9+%) from Sigma-Aldrich Co. and dichloromethane (CH_2Cl_2; 99.5+%) from Fluka, all of which were used without further purification. High-purity dinitrogen from Trigas was used to deoxygenate the solution before each electrochemical experiment. Tetra-*n*-butylammonium perchlorate (TBAP) was purchased from Fluka Chemika Co. and stored under vacuum at 40 °C prior to use. High-purity nitrogen was used to deoxygenate the solutions for at least 5 min before carrying out the electrochemical experiments. The supporting electrolyte was 0.1 M TBAP for cyclic voltammetry and 0.2 M TBAP for spectroelectrochemistry.

Other Physical Measurements. IR spectra were recorded on a Perkin-Elmer 783 in the range 4000−200 cm^{-1} (KBr pellets). Elemental analyses for C, H, and N were provided by the "Servizio di Microanalisi" at the Dipartimento di Chimica, Università "La Sapienza" (Rome), on an EA 1110 CHNS-O instrument. The ICP-PLASMA analysis of platinum was performed on a Varian Vista MPX CCD simultaneous ICP-OES.

Results and Discussion

Structural Features of Monometalated Dipyridinopyrazine Fragments and the Pt^{II} Complex $[(CN)_2Py_2PyzPtCl_2]$. It is well-documented in the literature that 2,3-di-2-pyridylpyrazine and its derivatives with annulated rings or open-chain substituents in the 5 and 6 positions (Chart 2A) are able to coordinate metal ions at the pyrazine and/or pyridine rings in a variety of fashions.[11−13] In most cases, the synthesis and physicochemical characterization of these complexes was given without precisely defining the coordination mode of the metal centers to the pyrazine or pyridine rings. However, X-ray work on some of the compounds unequivocally establishes that coordination of the metal ions can occur in a bidentate fashion either via one pyrazine and one pyridine N atom of the dipyridinopyrazine fragment (Ru^{II}, Co^{II}, Cu^{II}; "pyz−py" coordination, Chart 2B)[12] or via both N atoms of the two pyridine rings (Cu^{II}, Ni^{II}, Re^{V}; "py−py" coordination, Chart 2C).[13]

Prior to our recent single-crystal X-ray work on $[(CN)_2Py_2PyzPdCl_2]$, which showed "py−py" coordination of $PdCl_2$,[3] the only structurally characterized dipyridinopyrazine moieties containing bound Pd^{II} or Pt^{II} were, to our knowledge, the dichloro(6,7-dimethyl-2,

(8) Altomare, A.; Burla, M. C.; Cavalli, M.; Cascarno, G.; Giacovazzo, C.; Guagliardi, A.; Moliterni, A. G. G.; Polidori, G.; Spagna, R. *J. Appl. Crystallogr.* **1999**, *32*, 115.
(9) Sheldrick, G. M. *Acta Crystallogr.* **2008**, *A64*, 112.
(10) Lin, X. Q.; Kadish, K. M. *Anal. Chem.* **1985**, *57*, 1489.
(11) (a) Geary, W. J. *J. Chem. Soc. (A)* **1969**, 71. (b) Geary, W. J. *J. Chem. Soc. (A)* **1969**, 2118. (c) Geary, W. J.; Colton, D. F. *J. Chem. Soc. (A)* **1971**, 2457. (d) Cotton, D. F.; Geary, W. J. *J. Inorg. Nucl. Chem.* **1974**, *36*, 1499. (e) Colton, D. F.; Geary, W. J. *J. Chem. Soc., Dalton Trans.* **1972**, 547.
(12) (a) Rillema, D. P.; Taghdiri, D. G.; Jones, D. S.; Keller, C. D.; Worl, L. A.; Meyer, T. J.; Levy, H. A. *Inorg. Chem.* **1987**, *26*, 578. (b) Escuer, A.; Vicente, R.; Comas, T.; Ribas, J.; Gomez, M.; Solans, X.; Gatteschi, D.; Zanchini, C. *Inorg. Chim. Acta* **1991**, *181*, 51. (c) Gordon, K. C.; Al-Obaidi, A. H. R.; Jayaweera, P. M.; McGarvey, J. J.; Malone, J. F.; Bell, S. E. J. *J. Chem. Soc., Dalton Trans.* **1996**, 1591. (d) Rarig, R. S. Jr.; Hagrman, P. J.; Zubieta, J. *J. Solid State Sci.* **2002**, *4*, 77. (e) Chesnut, d. J.; Kusnetzov, A.; Birge, R. R.; Zubeita, J. *Inorg. Chem.* **1999**, *38*, 2663.
(13) (a) Escuer, A.; Comas, T.; Ribas, J.; Vicente, R.; Solans, X.; Zanchini, C.; Gatteschi, D. *Inorg. Chim. Acta* **1989**, *162*, 97. (b) Escuer, A.; Vicente, R.; Comas, T.; Ribas, J.; Gomez, M.; Solans, X. *Inorg. Chim. Acta* **1990**, *177*, 161. (c) Bandoli, G.; Gerber, T. I. A.; Jacobs, R.; du Preez, J. G. H. *Inorg. Chem.* **1994**, *33*, 178.

Chart 2

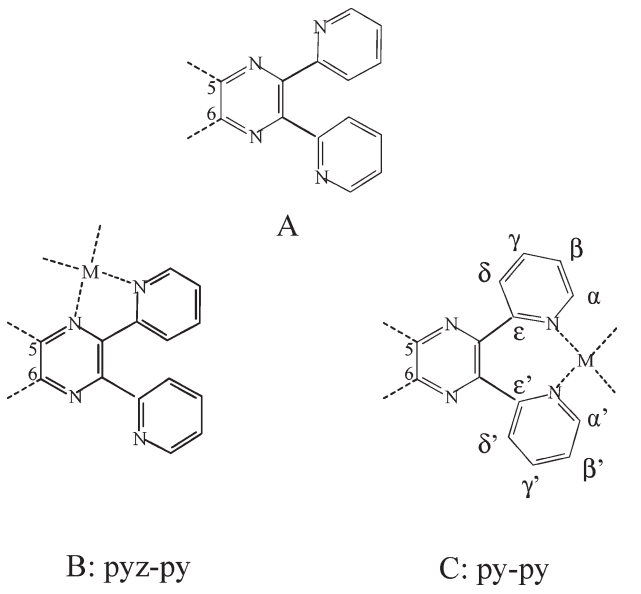

3-di-2-pyridylquinoxaline)palladium(II) complex,[14] the dichloro(6,7-dicyano-2,3-di-2-pyridylquinoxaline)palladium(II) complex,[15] and two Pt^{II} analogues in which the metal ions were coordinated in a "py−py" fashion.[16,17] This latter coordination contrasts with that of $[(dpq)PtCl_2]$ (dpq = 2,3-di-2-pyridyl-5,6-dihydropyrazine), where 2D ^1H NMR COSY spectra unequivocally indicate a "pyz−py" type of coordination.[17]

The Pt^{II} complex $[(CN)_2Py_2PyzPtCl_2]$ is isostructural with the corresponding Pd^{II} derivative,[3] and its structural properties along with ^1H NMR spectra are briefly described below. The metal center in $[(CN)_2Py_2PyzPtCl_2]$ displays a slightly tetrahedrally distorted square-planar coordination geometry provided by N atoms of the two pyridine rings and the chloride anions. The asymmetric unit contains $[(CN)_2Py_2PyzPtCl_2]$ and acetonitrile solvent molecules in the stoichiometric molar ratio of 2:1.75. ORTEP views of the two independent complex molecules (A, Pt1/Cl1/Cl2/N1−N6/C1−C16; B, Pt2/Cl3/Cl4/N7−N12/C17−C32) are shown in Figure 1 (molecule A) and Figure S2 (molecule B) in the SI, respectively. Selected bond distances and angles within the N_2PtCl_2 cores are listed in Table 2. The Pt−N [mean value 2.015(6) Å] and Pt−Cl [mean value 2.285(2) Å] bond lengths compare well with the mean values of 2.062 and 2.337 Å found in the Cambridge Crystallographic Databank for 1468 and 2794 entries, respectively.

The pyrazine rings of both independent complex molecules are substantially planar (maximum deviations of 0.0036 Å for atom C2 in molecule A and 0.012 Å for atom C17 in molecule B) and exhibit a complete delocalization of the double-bond system. The dihedral angles formed by the pyrazine ring with the mean plane through the

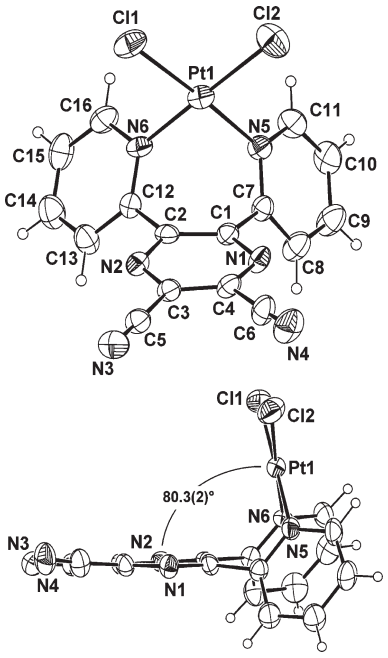

Figure 1. ORTEP front (top) and side (bottom) views (30% probability ellipsoids) of molecule A in $[(CN)_2Py_2PyzPtCl_2]$.

Table 2. Selected Bond Distances (Å) and Angles (deg) of $[(CN)_2Py_2PyzPtCl_2]$

Molecule A		Molecule B	
Pt1−N5	2.016(6)	Pt2−N11	2.006(6)
Pt1−N6	2.008(6)	Pt2−N12	2.031(7)
Pt1−Cl1	2.284(2)	Pt2−Cl3	2.284(2)
Pt1−Cl2	2.277(2)	Pt2−Cl4	2.294(2)
C1−C7	1.493(11)	C17−C23	1.507(12)
C2−C12	1.491(12)	C18−C28	1.453(13)
N6−Pt1−N5	86.9(2)	N11−Pt2−N12	87.2(3)
N6−Pt1−Cl2	177.49(17)	N11−Pt2−Cl3	178.07(19)
N5−Pt1−Cl2	91.21(17)	N12−Pt2−Cl3	91.3(2)
N6−Pt1−Cl1	89.85(16)	N11−Pt2−Cl4	90.49(18)
N5−Pt1−Cl1	176.64(19)	N12−Pt2−Cl4	177.4(2)
Cl2−Pt1−Cl1	92.10(9)	Cl3−Pt2−Cl4	91.00(8)

N_2PtCl_2 core are 80.3(2) and 87.0(2)° in A and B, respectively. The pyridine rings in each complex molecule are oriented nearly orthogonally, forming dihedral angles of 89.0(2) and 83.4(3)° in A and B, respectively. The pyz−py inter-ring average bond distance [1.486(12) Å] compares well with those found for the unmetalated $[(CN)_2Py_2Pyz]$ [1.482(4) Å] and palladated species $[(CN)_2Py_2PyzPdCl_2]$ [1.48(2) Å], which indicates unrelevant effects on such distances by metal coordination. The seven-membered chelation rings assume a boat conformation, with atoms Pt1, C1, C2 and Pt2, C17, C18 located above the plane of atoms N5, N6, C7, C12 (in A) and N11, N12, C23, C28 (in B), respectively. This geometry compares well with that reported for the related compounds dichloro(2,3-di-2-pyridylquinoxaline)platinum(II),[16] dichloro(6,7-dimethyl-2,3-di-2-pyridylquinoxaline)platinum(II),[17] and dichloro[2,5-diphenyl-3,4-bis(2-pyridyl)cyclopenta-2,4-dien-1-one]platinum(II) dichloromethane solvate.[18]

The molecules of the crystal are packed to form channels parallel to the crystallographic *a* axis hosting

(14) Nicole, F.; Cusumano, M.; Di Pietro, M. L.; Scopelliti, R.; Bruno, G. *Acta Crystallogr.* **1998**, *C54*, 485.
(15) Haas, M.; Liu, S.-X.; Neels, A.; Decurtins, S. *Eur. J. Org. Chem.* **2006**, *24*, 5467.
(16) Granifo, J.; Vargas, M. E.; Garland, M. T.; Baggio, R. *Inorg. Chim. Acta* **2000**, *305*, 143.
(17) Granifo, J.; Vargas, M. E.; Rocha, H.; Garland, M. T.; Baggio, R. *Inorg. Chim. Acta* **2001**, *321*, 209.
(18) Siemeling, U.; Scheppelmann, I.; Heinze, J.; Neumann, B.; Stammler, A.; Stammler, H.-G. *Chem.—Eur. J.* **2004**, *10*, 5661.

Table 3. ^{1}H NMR Parameters for $[(CN)_2Py_2Pyz]$, $[(CN)_2Py_2PyzPdCl_2]$, and $[(CN)_2Py_2PyzPtCl_2]$ in DMF-d_7 Solution

	$[(CN)_2Py_2Pyz]^a$			$[(CN)_2Py_2PyzPdCl_2]^a$			$[(CN)_2Py_2PyzPtCl_2]$		
	^{1}H (ppm)	m	J (Hz)	^{1}H (ppm)	m	J (Hz)	^{1}H (ppm)	m	J (Hz)
α^b	8.367	ddd	4.7, 1.6, 1.4	9.216	dd	5.7, 1.5	9.171	bd[c]	5.8
β^b	7.497	ddd	4.7, 7.1, 1.6	7.950	ddd	5.7, 7.7, 1.5	7.923	ddd	5.9, 7.5,1.4
γ^b	8.068	ddd	7.1, 7.6, 1.8	8.352	ddd	7.7, 7.7, 1.5	8.354	ddd	7.8, 7.8, 1.4
δ^b	8.093	ddd	7.6, 1.6, 1.3	8.027	h[d]		8.044	h[d]	

[a] Data taken from ref 3. [b] See Chart 2C. [c] bd = broad doublet. [d] h = hidden. The assignment was obtained by means of a ^{1}H−^{1}H COSY experiment.

Chart 3

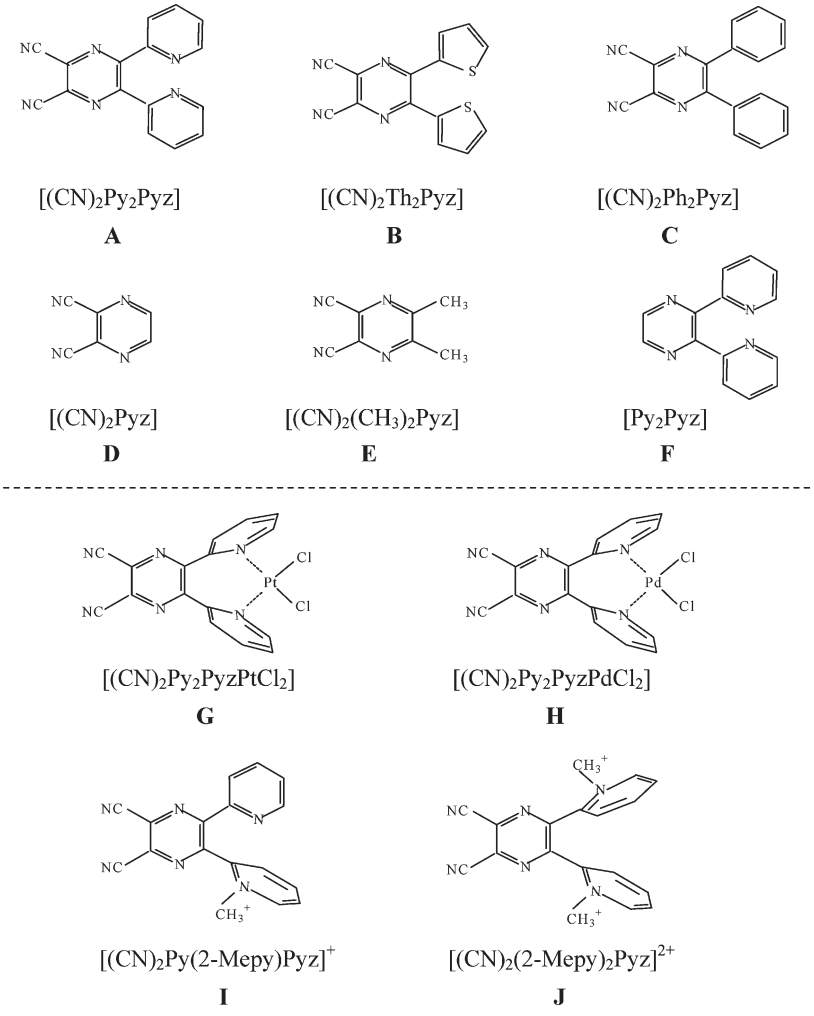

acetonitrile solvent molecules (Figure S3 in the SI). The crystal structure is stabilized by weak intra- and intermolecular C−H···N and C−H···Cl hydrogen-bonding interactions (see Table S3 in the SI).

The ^{1}H NMR spectral data of $[(CN)_2Py_2PyzPtCl_2]$ are reported in Table 3 along with previously published data on $[(CN)_2Py_2PyzPdCl_2]$ and $[(CN)_2Py_2Pyz]$[3] in DMF-d_7 for comparison. Examples of spectra are depicted in Figure S4 in the SI. The set of four resonance peaks common to all three species indicates equivalence of the two pyridine rings, an expected feature made evident by previous X-ray work on $[(CN)_2Py_2Pyz]$[1] and $[(CN)_2Py_2PyzPdCl_2]$,[3] along with the structure of the currently investigated Pt^{II} species. The binding of $PtCl_2$ to $[(CN)_2Py_2Pyz]$ leads to a low-field shift of all resonance peaks, as can be seen from the peak positions (ppm) of the α-, β-, γ-, and δ-type H atoms (Chart 2C) of the two pyridine rings. This is similar to what happens upon formation of $[(CN)_2Py_2PyzPdCl_2]$.[3]

Electrochemistry and Spectroelectrochemistry. Our discussion of the electrochemical and spectroscopic data will initially focus on the precursor $[(CN)_2Py_2Pyz]$ and related species (**A**−**F** in Chart 3), followed by a detailed analysis of the results for the $PtCl_2$ and $PdCl_2$ derivatives $[(CN)_2Py_2PyzPtCl_2]$ and $[(CN)_2Py_2PyzPdCl_2]$ (**G** and **H**) and of new data for two earlier reported[2c] cationic species, $[(CN)_2Py(2\text{-}Mepy)Pyz]^+$ and $[(CN)_2(2\text{-}Mepy)_2Pyz]^{2+}$ (**I** and **J**), which are obtained by mono- and diquaternization of the pyridine N atoms of the precursor $[(CN)_2Py_2Pyz]$.

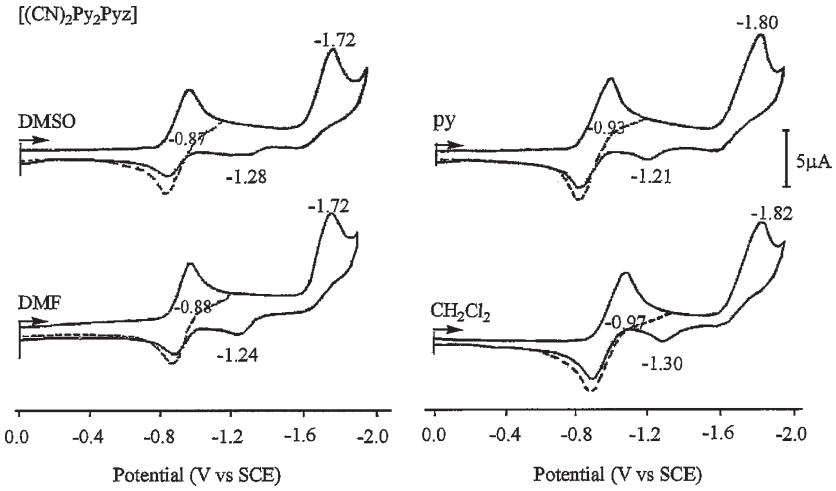

Figure 2. Cyclic voltammograms of $[(CN)_2Py_2Pyz]$ in DMSO, DMF, pyridine, and CH_2Cl_2, all containing 0.1 M TBAP. Scan rate 0.1 V s^{-1}.

Table 4. Half-Wave Potentials for the Reduction of $[(CN)_2Py_2Pyz]$ and Related Unmetalated Compounds in Nonaqueous Solvents Containing 0.1 M TBAP

			$E_{1/2}$, V vs SCE	
compound[a]		solvent	first reduction	second reduction
$[(CN)_2Py_2Pyz]$	**A**	DMSO	−0.87	−1.72[b]
		DMF	−0.88	−1.72[b]
		CH_2Cl_2	−0.97	−1.82[b]
		pyridine	−0.93	−1.80[b]
$[(CN)_2Th_2Pyz]$	**B**	pyridine	−0.93	−1.82[b]
$[(CN)_2Ph_2Pyz]$	**C**		−1.05	−1.92[b]
$[(CN)_2Pyz]$	**D**		−1.09	−1.54
$[(CN)_2(CH_3)_2Pyz]$	**E**		−1.34	−1.85
$[Py_2Pyz]$	**F**		−1.87	

[a] See Chart 3 for structures. [b] Peak potential at a scan rate of 0.1 V s^{-1}.

$[(CN)_2Py_2Pyz]$ (A) and Related Species (B−F). Cyclic voltammograms of the precursor $[(CN)_2Py_2Pyz]$ in four nonaqueous solvents are illustrated in Figure 2, and a summary of half-wave and peak potentials for each reduction process is given in Table 4. Upon scanning the potential from 0.0 to −2.0 V, one reversible reduction (at $E_{1/2} = -0.87$ to −0.97 V) and one irreversible reduction (at $E_{pc} = -1.72$ to −1.82 V) are obtained for a scan rate of 0.1 V s^{-1}. The cathodic peak currents for the two reductions are similar to each other in each solvent and involve stepwise one-electron additions, as described by eqs 1 and 2.

$$[(CN)_2Py_2Pyz] + e^- \rightleftharpoons [(CN)_2Py_2Pyz]^- \quad (1)$$

$$[(CN)_2Py_2Pyz]^- + e^- \rightleftharpoons [(CN)_2Py_2Pyz]^{2-} \rightarrow \text{products} \quad (2)$$

The second reduction of $[(CN)_2Py_2Pyz]$ involves a classical EC mechanism [an electron transfer (E) followed by a chemical reaction (C)] to give an unidentified product that is oxidized at $E_p = -1.21$ to −1.30 V on the return anodic sweep.

The $[(CN)_2Py_2Pyz]^-$ monoanion electrogenerated after the first one-electron addition in eq 1 is stable on the electrochemical and spectroelectrochemical time scales, and the UV−visible changes obtained as a function of time during controlled potential reduction in the thin-layer cell are shown in Figure 3.

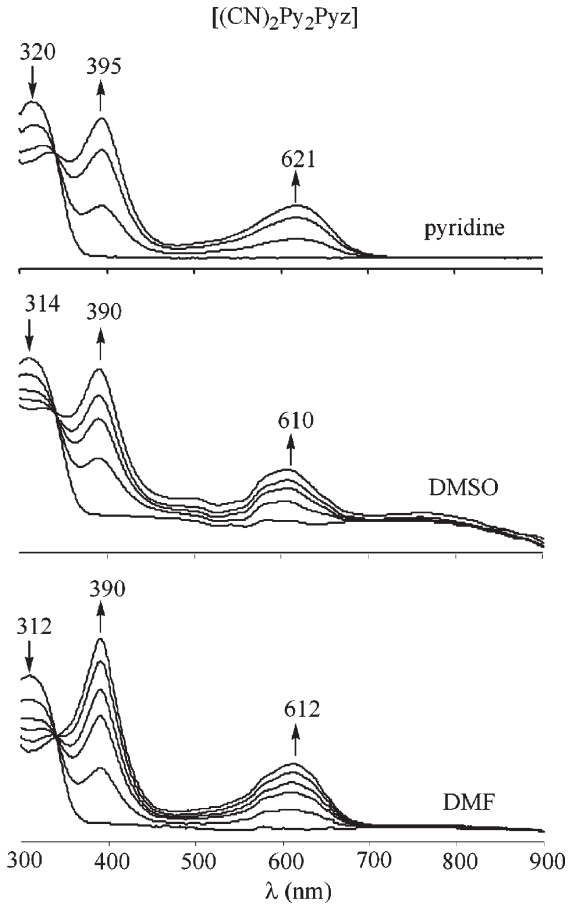

Figure 3. UV−visible spectral changes during the reversible controlled potential reduction of $[(CN)_2Py_2Pyz]$ to its $[(CN)_2Py_2Pyz]^-$ monoanion at an applied potential of −1.10 V.

Similar results are obtained in each solvent. While the unreduced compound is characterized by a single absorption band at 312−320 nm, assigned to a $\pi-\pi^*$ transition, the product of the one-electron addition has this band at 390−395 nm as a result of a lowering of the energy of the intraligand highest occupied molecular orbital (HOMO)−lowest unoccupied molecular orbital (LUMO) gap. Unexpectedly, an additional rather intense absorption is observed for the singly reduced species in

Table 5. UV−Visible Spectral Data (Range 300−800 nm) of Unmetalated Compounds before and after the First Reduction

			λ, nm (log ε)				
			initial		after the first reduction		
compound[a]		solvent					
$[(CN)_2Py_2Pyz]$	**A**	pyridine	320 (5.11)		323 (4.97)	395 (5.09)	621 (4.86)
		DMSO	314 (5.15)		314 (4.95)	390 (5.12)	610 (4.90)
		DMF	312 (5.19)		312 (4.91)	390 (5.26)	612 (4.85)
		CH_2Cl_2	314 (4.94)		314 (4.70)	392 (4.95)	610 (4.51)
$[(CN)_2Th_2Pyz]$	**B**	pyridine	317 (4.60)	390 (4.75)	317 (4.53)	402 (4.63)	623 (4.07)
$[(CN)_2Ph_2Pyz]$	**C**		340 (4.83)		340 (4.66)	389 (4.77)	621 (4.30)
$[(CN)_2Pyz]$	**D**		303 (4.26)		301 (4.50)	387 (4.10)	
$[(CN)_2(CH_3)_2Pyz]$	**E**		300 (4.51)		299 (5.02)	384 (4.67)	
$[Py_2Pyz]$	**F**		300 (4.59)		300 (4.47)	384 (4.37)	508 (4.61)

[a] See Chart 3.

the near-IR region (610−621 nm), which is reasonably assigned as $\pi_1^* \rightarrow \pi_2^*$, with the exact position depending upon the solvent (see Table 5). To the best of our knowledge, there are no reports in the literature for a one-electron-reduced unmetalated species carrying dipyridinopyrazine fragments, and thus there are no comparison compounds that might show a similar near-IR absorption (610−621 nm). The spectral changes in Figure 3 are reversible, and the UV−visible spectrum of unreduced $[(CN)_2Py_2Pyz]$ could be regenerated upon reoxidation at an applied potential of 0.00 V in a thin-layer cell (see Figure S5 in the SI). In each case, there is a well-defined isosbestic point at ~340 nm, indicating the lack of spectrally detectable intermediates during electrogeneration of $[(CN)_2Py_2Pyz]^-$.

In order to better understand the electrochemistry and spectroscopic data of $[(CN)_2Py_2Pyz]$ (**A**) in its neutral and singly reduced form, the redox and spectral behavior of the four dicyanopyrazine derivatives **B**−**E** (Chart 3) and 2,3-di-2-pyridylpyrazine, $[Py_2Pyz]$ (**F**), were also investigated in pyridine. Cyclic voltammograms of the five related compounds are shown in Figure 4, and a summary of half-wave and peak potentials is given in Table 4.

The shapes of the current−voltage curves for the thienyl (Th) and phenyl (Ph) compounds $[(CN)_2Th_2Pyz]$ and $[(CN)_2Ph_2Pyz]$ are similar to each other and also similar to that of the precursor $[(CN)_2Py_2Pyz]$. The observed identical value (−0.93 V) for the first electron addition in pyridine for the Py and Th derivatives does not hold perfectly if account is taken that the pyridine rings in the Py compound are electron-withdrawing, whereas the thienyl rings in the Th analogue, because of the presence of the electron-rich S atoms, are expected to behave oppositely, i.e., as electron donors, with an associated more negative value expected for the reduction potential, not observed. The cyclic voltammogram of the Ph compound, $[(CN)_2Ph_2Pyz]$, is also similar in shape to those of the Py and Th derivatives. For the Ph compound, the potentials for the two reductions (Figure 4) are shifted negatively by 100−120 mV, in better agreement with expectation. In fact, the two phenyl rings have definitely electron-donating properties, with this making electron uptake for the Ph compound a little more difficult. A reoxidation peak is obtained at $E_p = -1.34$ V after the second reduction of $[(CN)_2Ph_2Pyz]$ (see Figure 4), and this peak potential for this new reoxidation process is also negatively shifted from E_p for a similar reoxidation peak,

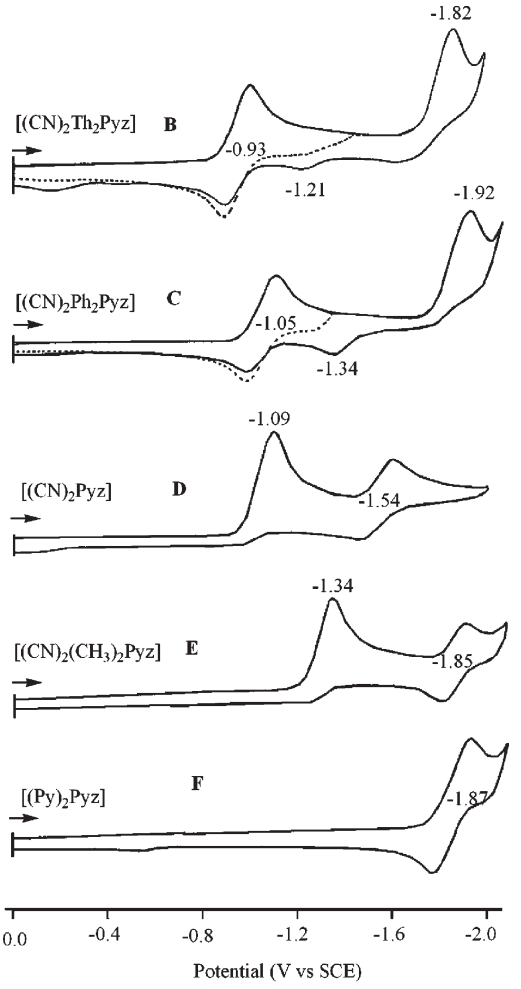

Figure 4. Cyclic voltammograms of related precursors in pyridine, 0.1 M TBAP. Scan rate 0.1 V s^{-1}.

which appears after generation of the doubly reduced Py and Th species.

Unlike the Py, Th, and Ph derivatives (**A**−**C**), the first reductions of **D** and **E** in pyridine are irreversible because of a coupled chemical reaction following the first electron transfer (see Figure 4). An irreversible reduction is also obtained in DMSO and CH_2Cl_2, the latter of which was utilized for variable-temperature measurements as low as −60 °C and remained irreversible, indicating a very fast chemical reaction following electron transfer. It should be

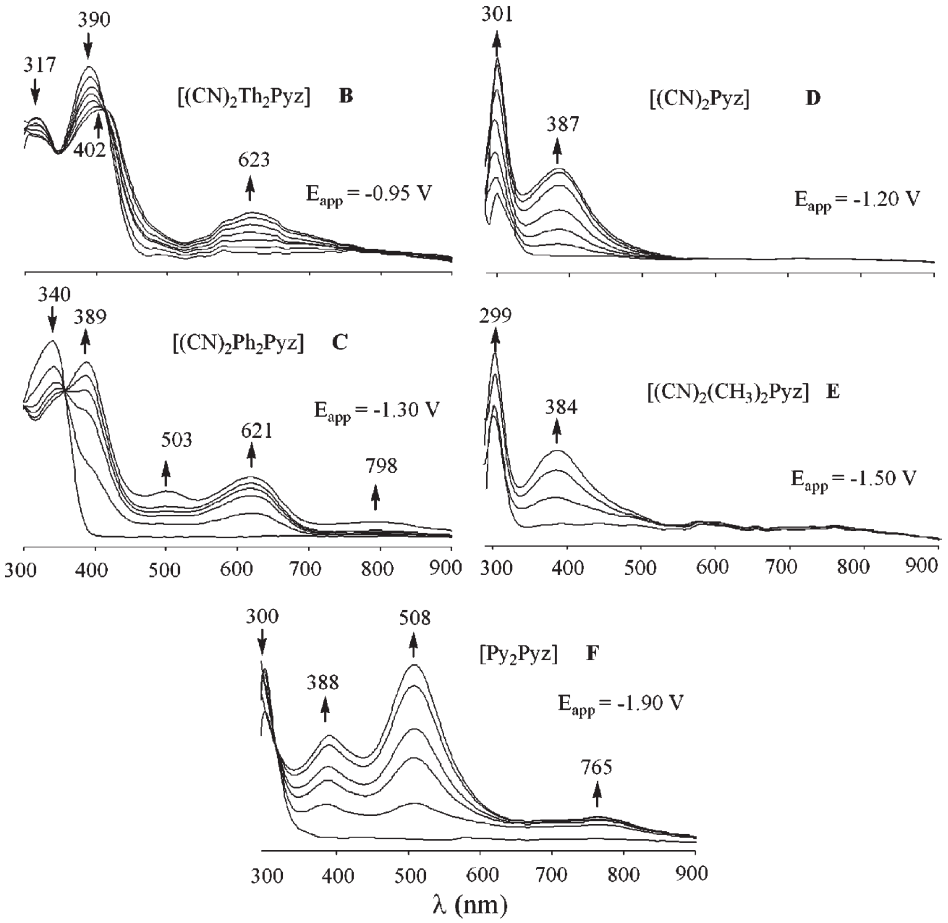

Figure 5. UV−visible spectral changes during the first reversible controlled potential reduction of $[(CN)_2Th_2Pyz]$, $[(CN)_2Ph_2Pyz]$, $[(CN)_2Pyz]$, $[(CN)_2(CH_3)_2Pyz]$, and $[Py_2Pyz]$ in pyridine, 0.2 M TBAP.

pointed out that the peak potential for the irreversible reduction of $[(CN)_2Pyz]$ is identical with the cathodic peak potential of −1.09 V for the reversible reduction of the Ph compound; it is also very close to peak potentials for reduction of the Py and Th compounds under the same experimental conditions. This strongly suggests that *the dicyanopyrazine moiety is the site of reduction*, with the exact potential being influenced by the type of ring substituent (Py, Th, Ph). The 250 mV negative shift in E_p for the reduction of **E** at the dicyanopyrazine moiety is consistent with the strong electron-donating nature of the two CH_3 groups. It is worth noting that cathodic peak currents for the first irreversible reduction of $[(CN)_2(CH_3)_2Pyz]$ and $[(CN)_2Pyz]$ are identical within experimental error to peak currents for the reversible reductions of the Py, Th, and Ph compounds at the same concentration and under the same solution conditions, thus indicating a one-electron-transfer step in each case. Finally, as seen in Figure 4, **F** is also reduced via a reversible one-electron-transfer step. This reaction occurs at $E_{1/2} = -1.87$ V and is negatively shifted by 940 mV from a similar reduction of $[(CN)_2Py_2Pyz]$, consistent with the absence of the highly electron-withdrawing CN groups. In summary, the first six compounds in Chart 3 (**A**−**F**) all undergo an initial one electron addition, but the ultimate reduction product is not the same in each case, as shown by the UV−visible spectra. In fact, three different types of spectra were obtained for the electrogenerated monoanions, one for the Py, Th, and Ph compounds (**A**−**C**), another for **D** and **E**, and a third for **F**. This is shown in Figure 5, which illustrates the time-resolved spectra under application of a controlled reduction potential.

As discussed above, the Py, Th, and Ph compounds share structural similarities in that each has five- or six-membered unsaturated rings in the 5 and 6 positions of pyrazine (see Chart 3). All three related compounds can also be reduced to a stable anion radical form as judged from the reversible cyclic voltammograms in Figures 2 and 4. The UV−visible spectra of the singly reduced Th and Ph derivatives are similar to each other (Figure 5) and also similar to that of the singly reduced precursor $[(CN)_2Py_2Pyz]$ (Figure 3) under identical experimental conditions. The reversible addition of one electron to the Th and Ph species results in a shift of absorptions in the region 300−400 nm ($\pi-\pi^*$) to lower energy and the appearance of broad intense absorptions with maxima at 621−623 nm ($\pi_1^*-\pi_2^*$). There are also weak absorptions at 503 and 798 nm for the Ph derivative.

As seen in Figures 3 and 5, UV−visible spectra of the singly reduced Py, Th, and Ph compounds are distinctly different from that of electroreduced dicyanopyrazine **D**. They also differ from that of the 5,6-dimethylated (**E**) species, and this can be accounted for by the presence of coupled chemical reactions following electron addition in the latter two compounds. The spectroelectrochemical data in Figure 3 and 5 also indicate that π-electron

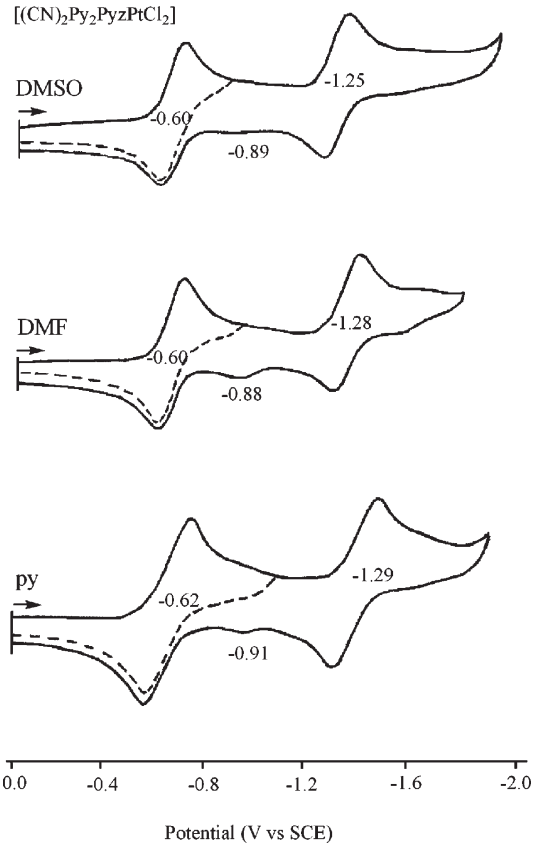

Figure 6. Cyclic voltammograms of $[(CN)_2Py_2PyzPtCl_2]$ in DMSO, DMF, and pyridine, 0.1 M TBAP.

delocalization in the monoanions $[(CN)_2Py_2Pyz]^-$, $[(CN)_2Th_2Pyz]^-$, and $[(CN)_2Py_2Pyz]^-$ is enhanced by the pyridine thienyl or phenyl rings at the 5 and 6 positions of the dicyanopyrazine moiety. This contrasts with the cases of **D** and **E**, the first of which has no substituents at the 5 and 6 positions and the second of which contains methyl groups, which do not contribute to stabilization of the monoanion. Although the spectra of electroreduced $[(CN)_2Pyz]$, $[(CN)_2(CH_3)_2Pyz]$, and **F** are presented in Figure 5, the absorbing species represent side products of a chemical reaction and were not examined in further detail.

$[(CN)_2Py_2PyzPtCl_2]$. Cyclic voltammograms of the monoplatinated precursor $[(CN)_2Py_2PyzPtCl_2]$ (Chart 3) in DMSO, DMF, and pyridine are shown in Figure 6. Two reversible one-electron reductions are obtained in each solvent at almost identical potentials. It is worth noting that the first electron addition at $E_{1/2} = -0.60$ to -0.62 V is easier than that for reduction of the parent unmetalated compound (Figure 2 and Table 6) by about 300 mV, with the facilitated process clearly being due to the electron-withdrawing effect of the $PtCl_2$ groups after coordination to the precursor $[(CN)_2Py_2Pyz]$. Doubly reduced $[(CN)_2Py_2PyzPtCl_2]^{2-}$ ($E_{1/2} = -1.25$ to -1.29 V) is also significantly easier to generate and more stable than the doubly reduced parent compound ($E_p = -1.72$ to -1.80 V), indicating that coordination of $PtCl_2$ favors charge redistribution and stabilization within the entire molecule. These data are strongly reminiscent of what was reported for the "pyrazinoporphyrazine" complex $[(PdCl_2)_4Py_8TPyzPzPd]$ (see Chart 1A for the unmetalated macrocycle),

Table 6. Comparison of Half-Wave Potentials for Reduction of the Investigated Compounds in Pyridine, DMSO, DMF, and CH_2Cl_2 Containing 0.1 M TBAP

			$E_{1/2}$, V vs SCE		
type	solvent	compound	first	Δ^a	second
precursors	DMSO	$[(CN)_2Py_2Pyz]$	−0.87		−1.72[b]
		$[(CN)_2Py_2PyzPdCl_2]$	−0.54[b]	0.33	[c]
		$[(CN)_2Py_2PyzPtCl_2]$	−0.60	0.27	−1.25
		$[(CN)_2Py(2\text{-}Mepy)Pyz]^{+}$ [d]	−0.60	0.27	−0.79
		$[(CN)_2(2\text{-}Mepy)_2Pyz]^{2+}$ [d]	−0.36	0.51	−0.57
	DMF	$[(CN)_2Py_2Pyz]$	−0.88		−1.72[b]
		$[(CN)_2Py_2PyzPdCl_2]$	−0.56[b]	0.31	[c]
		$[(CN)_2Py_2PyzPtCl_2]$	−0.60	0.28	−1.28
	CH_2Cl_2	$[(CN)_2Py_2Pyz]$	−0.97		−1.82[b]
		$[(CN)_2Py_2PyzPdCl_2]$	−0.60	0.37	
		$[(CN)_2Py_2PyzPtCl_2]$	−0.65	0.32	−1.35
	pyridine	$[(CN)_2Py_2Pyz]$	−0.93		−1.80[b]
		$[(CN)_2Py_2PyzPtCl_2]$	−0.62	0.31	−1.29
macrocycles	DMSO[e]	$[Py_8TPyzPzPd]$	−0.26		−0.60
		$[(PdCl_2)_4Py_8TPyzPzPd]$	0.00	0.26	−0.37
		$[(2\text{-}Mepy)_8TPyzPzPd]^{8+}$	0.08	0.34	−0.33
	DMF[e]	$[Py_8TPyzPzPd]$	−0.25		−0.59
		$[(PdCl_2)_4Py_8TPyzPzPd]$	0.04	0.29	−0.37
		$[(2\text{-}Mepy)_8TPyzPzPd]^{8+}$	0.12	0.37	−0.48

[a] Difference in potentials between $E_{1/2}$ or E_p for first reductions and that of the parent compound $[(CN)_2Py_2Pyz]$ or $[Py_8TPyzPzPd]$. [b] Peak potential at a scan rate of 0.1 V s^{-1}. [c] Additional reductions after loss of the $PdCl_2$ group are not shown (see Figure 8). [d] Data taken from ref 2c. [e] Data taken from ref 3.

which is substantially easier to reduce than the parent mononuclear complex $[Py_8TPyzPzPd]$ as a result of externally coordinated $PdCl_2$ units.[3]

A comparison of the electrochemical data in Table 6 for $[(CN)_2Py_2Pyz]$ with published data for the related mononuclear macrocycle $[Py_8TPyzPzPd]$[3] shows that in each case the larger macrocycle is easier to reduce than the precursor by more than 600 mV, with the exact magnitude of the difference depending upon the solvent.

The best defined cyclic voltammograms and the most stable electroreduction products of $[(CN)_2Py_2PyzPtCl_2]$ are obtained in DMSO, but as in the case of the unmetalated precursors, a chemical reaction occurs after the second reduction, as evidenced by the appearance of a reoxidation peak at $E_p = -0.88$ to -0.91 V on the reverse potential scan (see Figure 6). The "new" anodic peak occurs only after the addition of a second electron to the compound and is located at potentials 300−390 mV positive of E_p for a similar reoxidation peak in the case of the unmetalated parent species (see Figure 2). The absolute potential separation in anodic peak potentials between the chemically generated product of the second electron addition to $[(CN)_2Py_2PyzPtCl_2]$ and $[(CN)_2Py_2Pyz]$ ranges from 300 to 390 mV in the different solvents and is similar to the absolute potential difference between $E_{1/2}$ values for the first reversible reduction of the same two compounds under the given solution conditions. This result suggests that $PtCl_2$ is retained on the molecule after the second electron transfer.

Like in the case of the parent unmetalated compound, UV−visible spectra were obtained after each one-electron reduction of $[(CN)_2Py_2PyzPtCl_2]$ in a thin-layer cell, and these spectral changes as a function of time in three of the solvents are illustrated in Figures 7 (first reduction) and S6 (second reduction) in the SI. The first reduction is spectrally reversible (see Figure S7 in the SI), and similar

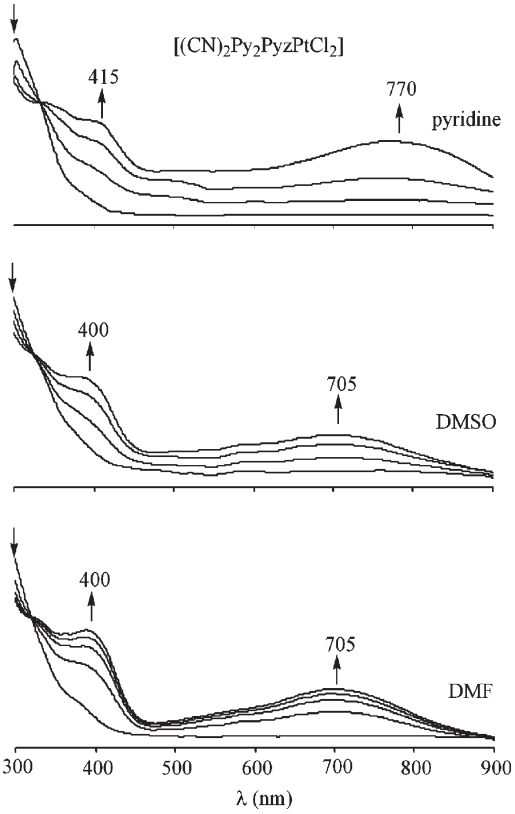

Figure 7. UV−visible spectral changes during the reversible controlled potential reduction of $[(CN)_2Py_2PyzPtCl_2]$ to its monoanionic form at an applied potential of −0.80 V in the three solvents containing 0.2 M TBAP.

spectra are obtained for the electrogenerated monoanion $[(CN)_2Py_2PyzPtCl_2]^-$ in the three solvents; there is a band at 400−415 nm, assigned to the intraligand HOMO−LUMO $\pi-\pi^*$ transition, only slightly moved to lower energy with respect to that of the unmetalated precursor (390−395 nm, Figure 3). Much broader absorptions are present in the lower energy region of the spectrum (500−900 nm), with a maximum intensity at ∼770 nm (pyridine) or 705 nm (DMSO and DMF). The marked shift to lower energy of these near-IR envelopes for the monoanionic platinated species as compared to that of the singly reduced parent compound is obviously a result of platination and implies a rearrangement of the excited energy levels. It is possible that the broad 500−900 nm envelope might result from the overlap of $\pi_1 \rightarrow \pi_2^*$ and possibly also metal-to-ligand charge-transfer (MLCT) bands. The examined compounds carrying metalated dipyridinopyrazine fragments have evidenced in their unreduced form such MLCT bands prevalently in the range 400−550 nm,[12a,19,20] also exceeding this range,[21] but no information is available for their corresponding monoanions.

$PtCl_2$ in the absence of the precursor is irreversibly reduced at $E_p = -1.75$ to -1.79 V in py, DMF, or DMSO (see Figure S8 in the SI), and this process is not seen in the cyclic voltammograms of Figure 6. Thus, there is no electrochemical evidence for the dissociation of bound

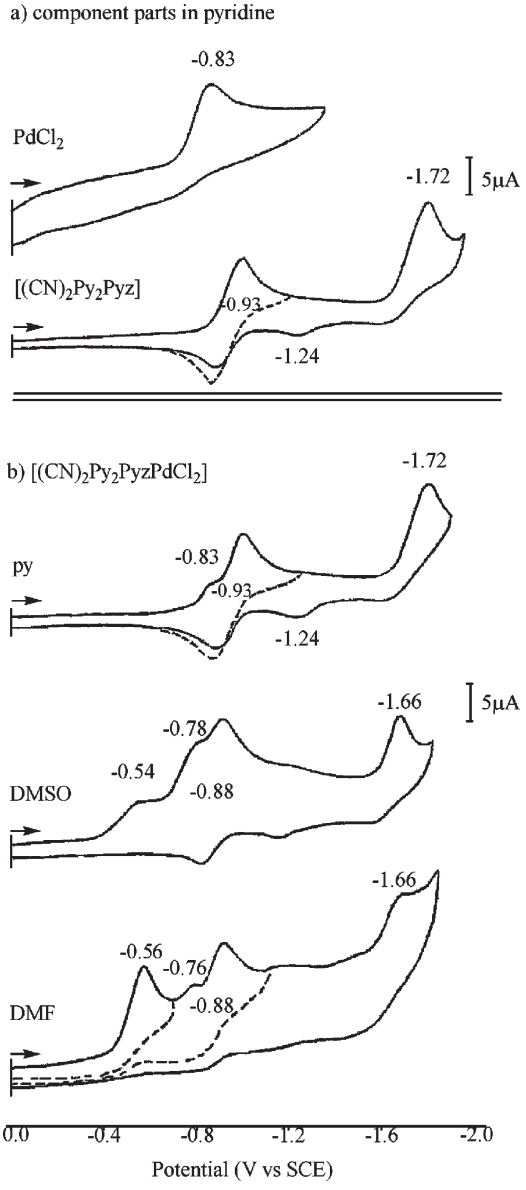

Figure 8. Cyclic voltammograms of (a) $PdCl_2$ and $[(CN)_2Py_2Pyz]$ in py and (b) $[(CN)_2Py_2PyzPdCl_2]$ in the three nonaqueous solvents containing 0.1 M TBAP. Scan rate 0.1 V s^{-1}.

$PtCl_2$ from $[(CN)_2Py_2PyzPtCl_2]$, nor is there any spectral evidence that the electroactive $PtCl_2$ unit is reduced while coordinated to $[(CN)_2Py_2PyzPtCl_2]$, as is the case for bound $PdCl_2$, whose electrochemistry is described on the following pages.

In summary, two electrons can be reversibly added to $[(CN)_2Py_2PyzPtCl_2]$ in the utilized nonaqueous solvents, and these reactions are given by eqs 3 and 4. The second-reduction product is moderately stable in DMSO but undergoes a small amount of decomposition or side reaction in py and DMF.

$$[(CN)_2Py_2PyzPtCl_2] + e^- \rightleftharpoons [(CN)_2Py_2PyzPtCl_2]^- \quad (3)$$

$$[(CN)_2Py_2PyzPtCl_2]^- + e^- \rightleftharpoons [(CN)_2Py_2PyzPtCl_2]^{2-} \quad (4)$$

$[(CN)_2Py_2PyzPdCl_2]$. The most straightforward electrochemistry of $[(CN)_2Py_2PyzPdCl_2]$ is shown in

(19) Rumisnki, R.; Cambron, R. T. *Inorg. Chem.* **1990**, *29*, 1575.
(20) Baiano, J. A.; Carlson, D. L.; Wolosh, G. M.; DeJesus, D. E.; Knowles, C. F.; Szabo, E. G.; Murphy, W. R. Jr. *Inorg. Chem.* **1990**, *29*, 2327.
(21) Brewer, K. J.; Murphy, W. R. Jr.; Petersen, J. D. *Inorg. Chem.* **1987**, *26*, 3376.

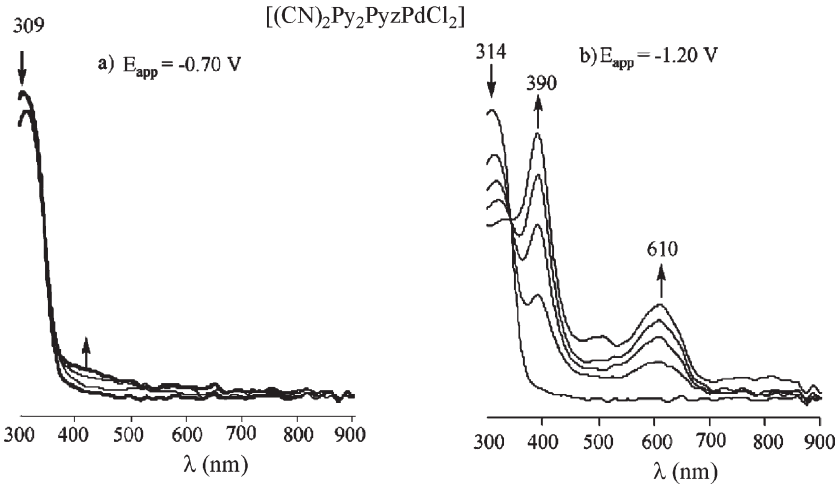

Figure 9. UV−visible spectral changes during controlled potential reduction of $[(CN)_2Py_2PyzPdCl_2]$ in DMSO at (a) −0.70 V and (b) −1.20 V, containing 0.2 M TBAP.

Figure 8b, where three reductions are observed in pyridine and located at the same potentials as those for reduction of the individual redox-active components under these solution conditions, i.e, −0.83 V for $PdCl_2$ and −0.93 and −1.72 V for $[(CN)_2Py_2Pyz]$ (Figure 8a). This is consistent with a loss of the electroactive $PdCl_2$ group upon dissolving the compound in pyridine. A loss of coordinated $PdCl_2$ units was also reported to occur for the related pentapalladated porphyrazine complex $[(PdCl_2)_4Py_8TPyzPzPd]$.[3]

Quite different electrochemical results are observed in DMSO and DMF, as seen by the voltammograms in Figure 8b. Under these solution conditions, the first reduction is irreversible and located at $E_p = -0.54$ V (DMSO) or −0.56 V (DMF) for a scan rate of 0.1 V s^{-1}. Both electron transfers are easier by more than 300 mV, as compared to the first reduction of unmetalated $[(CN)_2Py_2Pyz]$. A potential similar to that for reduction of $[(CN)_2Py_2PyzPtCl_2]$, $E_{1/2} = -0.60$ V (see Table 4), is also measured.

The main difference between the precursors containing bound $PtCl_2$ and bound $PdCl_2$ is that a fast chemical reaction follows electroreduction of $[(CN)_2Py_2PyzPdCl_2]$, giving an overall irreversible electrochemical process, but this does not occur for $[(CN)_2Py_2PyzPtCl_2]$, where the electrogenerated anion radical is stable on the cyclic voltammetric and spectroelectrochemical time scales (see Figures 6 and 7).

The similarity in the first-reduction potentials of $[(CN)_2Py_2PyzPdCl_2]$ and $[(CN)_2Py_2PyzPtCl_2]$ in either DMSO or DMF is consistent with a similar site of electron transfer in both molecules, and this we assign at the conjugated π system because $PtCl_2$ reduction itself occurs at a very negative potential of −1.58 V in DMSO or −1.79 V in DMF (see Figure S8 in the SI). The chemical reaction following electron addition to $[(CN)_2Py_2PyzPdCl_2]$ is consistent with a loss of the palladium fragment after the formation of Pd^I and Pd^0 species,[22] after which the uncomplexed parent compound

Scheme 1. Proposed ECEC Mechanism for Reduction of $[(CN)_2Py_2PyzPdCl_2]$

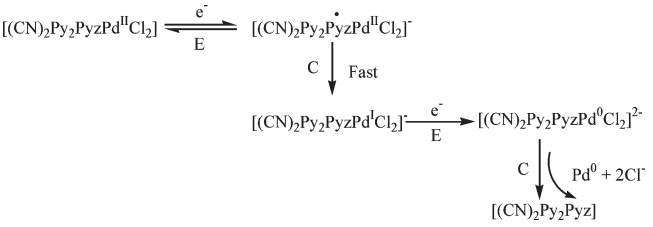

undergoes reduction at $E_{1/2} = -0.88$ V and $E_p = -1.66$ V, as seen in Figure 8b.

The fact that the peak currents for the first two reductions of $[(CN)_2Py_2PyzPdCl_2]$ are similar to each other in DMSO suggests that the same number of electrons are transferred in each step and leads to the electrochemical ECEC mechanism shown in Scheme 1. The first electron addition at $E_p = -0.54$ V is proposed to occur at the π ring system of the compound (E). This is then followed by a fast chemical reaction to give a Pd^I derivative (C), which is further reduced in a second step at $E_p = -0.78$ V in DMSO to give Pd^0 (E), after which a chemical dissociation step occurs (C) to give the unreduced parent compound that can be further reduced as described above.

Additional supporting evidence for the mechanism shown in Scheme 1 is given by UV−visible spectra measured during controlled potential reduction of $[(CN)_2Py_2PyzPdCl_2]$ in a thin-layer cell. These spectra are shown in Figure 9. The cyclic voltammogram in Figure 8b indicates a global one electron addition at $E_p = -0.54$ V, but only small changes in the UV−visible spectra are seen upon application of a controlled reduction potential of −0.70 V (Figure 9a). This lack of spectral change is consistent with a $Pd^{II/I}$ process at $E_p = -0.54$ V (as opposed to reduction at the conjugated π system). A similar potential of $E_{1/2} = -0.51$ V has been reported for the $Pd^{II/I}$ reaction of $Pd(dppx)_2(BF_4)_2$ in CH_2Cl_2 where dppx = 1,2-bis(diphenylphosphinomethyl)benzene.[22]

Further controlled potential reduction of $[(CN)_2Py_2PyzPdCl_2]$ at −1.20 V in DMSO should generate Pd^0 and the parent compound, which would be reduced to its monoanionic form at $E_{1/2} = -0.88$ V. This seems to be

(22) Miedaner, A.; Haltiwanger, R. C.; Dubois, D. L. *Inorg. Chem.* **1991**, *30*, 417.

what occurs because the final spectrum in Figure 9b after reduction at −1.20 V is identical with the spectrum of $[(CN)_2Py_2Pyz]^-$ electrogenerated from $[(CN)_2Py_2Pyz]$ in the absence of $PdCl_2$ (Figure 3), thus adding further support for the proposed mechanism in DMSO.

An electrochemical ECE mechanism is also proposed to occur for reduction of $[(CN)_2Py_2PyzPdCl_2]$ in DMF, but in this solvent, the two one-electron-transfer steps ($Pd^{II/I}$ and $Pd^{I/0}$) are merged into a single process located at $E_p = -0.56$ V for a scan rate of 0.1 V s^{-1}. This would imply a chemical reaction different from that in DMSO or maybe a faster reaction.

Proof for the initial ECE process in DMF is given by analysis of the peak potential and peak current for the first reduction as a function of the potential scan rate. The reduction peak has the shape of a reversible one-electron transfer followed by an irreversible chemical reaction,[23] i.e., $|E_p - E_{p/2}| = 0.060$ V (see Figure S9a in the SI), but the peak current is almost double that for the first electron addition in DMSO (Figure 8b). In addition, a diagnostic plot of E_p versus the log of scan rate should be equal to $-0.030/n$ for an EC mechanism of the type[23] described in Scheme 1, where n is the number of electrons transferred in the rate-determining step. This indeed is observed, as shown in Figure S9b in the SI, where the slope of the plot is −0.03 V, consistent with $n = 1$. In summary, the reduction of $[(CN)_2Py_2PyzPdCl_2]$ in DMF proceeds via an initial rate-determining one-electron transfer followed by an irreversible chemical reaction and a second electron addition at the same potential as the first.

It was anticipated that controlled potential reduction of $[(CN)_2Py_2PyzPdCl_2]$ at −0.70 V in DMF would lead to a loss of $PdCl_2$ in the first multielectron-transfer step with subsequent formation of the parent compound, but this is not the case, as indicated by the spectroelectrochemical data shown in Figure S10 in the SI. The UV−visible spectrum of the species produced during reduction at −0.70 V has bands at 414 and 620 nm and resembles the UV−visible spectrum of doubly reduced $[(CN)_2Py_2PyzPtCl_2]^{2-}$, which has bands at 413 and ∼600 nm in DMF (Figure S6 in the SI). The 414 nm band further increases in intensity after controlled potential reduction at −1.20 V, and the absence of any bands that can be reasonably assigned to the singly reduced parent compound (λ = 390 and 610 nm) suggests the formation of a new chemical species on the spectroelectrochemical but not cyclic voltammetric time scale where $[(CN)_2Py_2Pyz]$ and $[(CN)_2Py_2Pyz]^-$ are observed. The identity of the species chemically generated after reduction of $[(CN)_2Py_2PyzPdCl_2]$ in DMF was not further characterized because it was not of central importance to this study.

$[(CN)_2Py(2\text{-}Mepy)Pyz]^+$ and $[(CN)_2(2\text{-}Mepy)_2Pyz]^{2+}$ Cations. It was earlier pointed out that quaternization of the eight pyridine N atoms on the mononuclear palladium(II) porphyrazine macrocycle $[Py_8TPyzPzPd]$ led to the octacationic complex $[(2\text{-}Mepy)_8TPyzPzPd]^{8+}$, which was reduced at a potential definitely more positive than that of the neutral species but even more positive (slightly) than that of the compound obtained after exocyclic coordination on the unligated compound by $PdCl_2$.[3] Specifically, the positive shift in $E_{1/2}$ (see the bottom of Table 6) upon going from $[Py_8TPyzPzPd]$ to $[(PdCl_2)_4TPyzPzPd]$ is 260 mV in DMSO and 290 mV in DMF as compared to 340 and 390 mV, respectively, upon going from $[Py_8TPyzPzPd]$ to $[(2\text{-}Mepy)_8TPyzPzPd]^{8+}$ under the same solution conditions.[3] Thus, there is little difference in this respect between the porphyrazine macrocycle with four externally coordinated $PdCl_2$ units and the smaller precursor with just one.

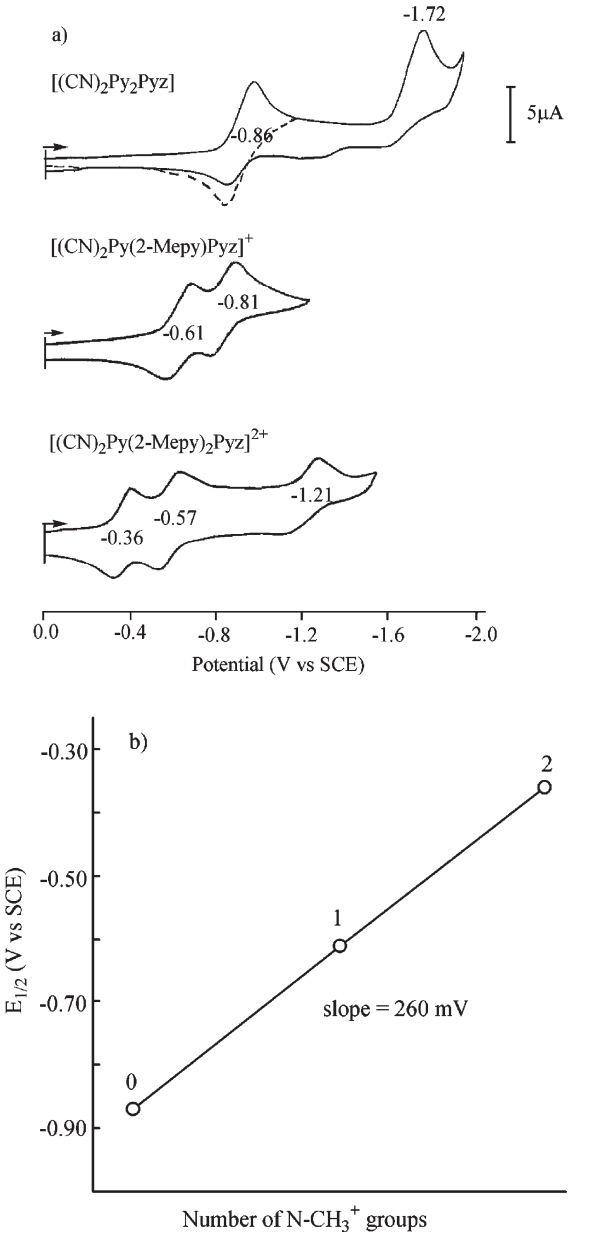

Figure 10. (a) Cyclic voltammograms of $[(CN)_2Py_2Pyz]$, $[(CN)_2Py(2\text{-}Mepy)Pyz]^+$, and $[(CN)_2(2\text{-}Mepy)_2Pyz]^{2+}$ in DMSO, 0.1 M TBAP. Scan rate 0.1 V s^{-1}. (b) Plot of $E_{1/2}$ for the first reduction versus the number of $N-CH_3^+$ groups on the compound. Potentials for the $N-CH_3^+$ derivatives are taken from ref2c.

Positive shifts in $E_{1/2}$ are also seen in the present study upon going from $[(CN)_2Py_2Pyz]$ to $[(CN)_2Py_2PyzPtCl_2]$ or from $[(CN)_2Py_2Pyz]$ to $[(CN)_2Py_2PyzPdCl_2]$, and this is evident from the data in Table 6, where the difference in the positive potential shift with respect to the parent compound is indicated by the symbol Δ and amounts to 270−280 mV in the case of the $PtCl_2$ species, where

(23) Nicholson, R. S.; Shain, I. *Anal. Chem.* **1964**, *36*, 706.

meaningful thermodynamic comparisons can be made for the reversible first reductions.

The difference in the first reduction potential between $[(PdCl_2)_4Py_8TPyzPzPd]$ ($E_{1/2}$ = 0.00 V) and $[(2\text{-Mepy})_8TPyzPzPd]^{8+}$ ($E_{1/2}$ = 0.08 V) amounts to only 80 mV in DMSO, with the quaternized compound being slightly easier to reduce. In contrast, $[(CN)_2Py_2PyzPtCl_2]$ and $[(CN)_2Py(2\text{-Mepy})Pyz]^+$ are reduced at identical half-wave potentials of −0.61 V in DMSO (see Table 6), but a larger shift in $E_{1/2}$ occurs upon going from $[(CN)_2Py_2Pyz]$ to $[(CN)_2(2\text{-Mepy})_2Pyz]^{2+}$, where the potential difference between $E_{1/2}$ for formation of the two anion radicals amounts to 510 mV. Also, as seen in Figure 10, a linear relationship exists between $E_{1/2}$ of the first reduction and the number of $N-CH_3^+$ groups on the compound, with the ease of reduction following the order $[(CN)_2(2\text{-Mepy})_2Pyz]^{2+}$ (−0.36 V) > $[(CN)_2Py(2\text{-Mepy})Pyz]^+$ (−0.61 V) > $[(CN)_2Py_2Pyz]$ (−0.87 V). $E_{1/2}$ for the second reduction of the two quaternized compounds also depends on the number of $N-CH_3^+$ groups, but a comparison with $[(CN)_2Py_2Pyz]$ was not possible because of the chemical reaction following the second electron transfer of the parent compound.

Conclusions

One main goal of this study was to better understand the electrochemistry of tetrakis[5,6-di(2-pyridyl)-2,3-pyrazino]-porphyrazines of the types $[Py_8TPyzPzH_2]$ and $[Py_8TPyzPzM]$.[1,2a,2c] We previously demonstrated that electron uptake by the macrocycle could be facilitated by hundreds of millivolts after quaternization of the pyridine N atoms of $[Py_8TPyzPzM]$, giving the octacationic species $[(2\text{-Mepy})_8TPyzPzM]^{8+}$.[2c] A similar facilitation of electron uptake could be achieved by external metal coordination at the pyridyl N atoms, and this was demonstrated for the case of pentanuclear species $[(PdCl_2)_4Py_8TPyzPzPd]$, which could be converted to a stable anion radical at potentials close to 0.00 V vs SCE.[3]

The four dipyridinopyrazine units on $[Py_8TPyzPzH_2]$ are themselves electroactive in the absence of the porphyrazine macrocycle, and it was therefore of interest to elucidate how their electrochemistry might be modified by systematic changes in the pyrazine substituents or by metal coordination at the pyridyl N atoms in a manner similar to that observed for the larger macrocycle, in this case $[(PdCl_2)_4Py_8TPyzPzPd]$. This was examined in the present study, where we first characterized the electrochemistry of $[(CN)_2Py_2Pyz]$, a precursor for the larger macrocycle, as well as five related pyrazine derivatives having different electron-donating or electron-withdrawing ring substituents and then related results on these compounds to that of two metalated analogues, $[(CN)_2Py_2PyzPtCl_2]$, which was synthesized for the first time in this study, and $[(CN)_2Py_2PyzPdCl_2]$, which was previously synthesized but not electrochemically characterized.[3]

The ligation of $PtCl_2$ or $PdCl_2$ units to the pyridine N atoms of precursor $[(CN)_2Py_2Pyz]$ results in an easier first and second one-electron reduction, as shown by their more positive potential values, and a parallel electrochemical behavior is observed when the precursor is changed to its corresponding mono- and diquaternized cations, $[(CN)_2Py(2\text{-Mepy})Pyz]^+$ and $[(CN)_2(2\text{-Mepy})_2Pyz]^{2+}$. Thus, either metalation or quaternization of $[(CN)_2Py_2Pyz]$ parallel that reported for the pentanuclear pyrazinoporphyrazine $[(PdCl_2)_4Py_8TPyzPzPd]$ and the octacation $[(2\text{-Mepy})_8TPyzPzPd]^{8+}$ as compared to the related mononuclear species, $[Py_8TPyzPzPd]$.

These results are of interest because they demonstrate an effective π-electronic contact between the peripheral heteroatomic fragments and the dicyanopyrazine moiety, although the pyridine rings involved in "py−py" metalation or N-pyridine quaternization are in both cases considerably displaced out of the plane of the pyrazine ring. Also, as shown by the electrochemical and spectral data in pyridine, the dicyanopyrazine moiety is the site of reduction in $[(CN)_2Py_2Pyz]$ as well as the related dicyanopyrazine derivatives carrying thienyl or phenyl substituents in the 5 and 6 positions of pyrazine. The one-electron-reduced species of all three compounds is stable on the spectroelectrochemical time scale and is characterized by the presence of intense near-IR absorptions assigned as $\pi_1^* \rightarrow \pi_2^*$ transitions. Broad absorptions in the region 500−900 nm are also present in spectra of the 1− charged platinated species $[(CN)_2Py_2PyzPtCl_2]^-$ and its palladated analogue $[(CN)_2Py_2PyzPdCl_2]^-$, and they are tentatively attributed to the concomitant presence of $\pi_1^* \rightarrow \pi_2^*$ and MLCT transitions.

Acknowledgment. Financial support by the Robert A. Welch Foundation (Grant E-680 to K.M.K.) and the University of "La Sapienza" and MIUR (PRIN 2007XWBRR4 to C.E.) is gratefully acknowledged. Thanks are expressed to Prof. L. Mannina for NMR spectra and useful discussions.

Supporting Information Available: X-ray crystal data in CIF format, IR spectrum of $[(CN)_2Py_2PyzPtCl_2]$ (Figure S1); details of the X-ray data collection and structure analysis (Figures S2 and S3), ^1H NMR spectra of $[(CN)_2Py_2Pyz]$, $[(CN)_2Py_2PyzPdCl_2]$, and $[(CN)_2Py_2PyzPtCl_2]$ (Figure S4); UV−visible spectral changes of $[(CN)_2Py_2Pyz]$, $[(CN)_2Py_2PyzPtCl_2]$, and $[(CN)_2Py_2PyzPdCl_2]$ (Figures S5−S7 and S10); Tables S1−S3 containing experimental data and relevant conformational parameters of $[(CN)_2Py_2PyzPtCl_2]$; cyclic voltammograms of $PtCl_2$ in py, DMSO, and DMF (Figure S8); cyclic voltammograms of the first reduction of $[(CN)_2Py_2PyzPdCl_2]$ and plot of E_p for the first reduction versus different scan rates (Figure S9). This material is available free of charge via the Internet at http://pubs.acs.org. CCDC 696860 contains the supplementary crystallographic data for this paper. The atomic coordinates for this structure have been deposited with the Cambridge Crystallographic Data Centre. The coordinates can be obtained, upon request, from the Director, Cambridge Crystallographic Data Centre, 12 Union Road, Cambridge CB2 1EZ, U.K.